



Mucociliary Transit Assessment Using Automatic Tracking in Phase Contrast X-Ray Images of Live Mouse Nasal Airways

Hye-Won Jung¹ · Ivan Lee¹ · Sang-Heon Lee¹ · Kaye Morgan² · David Parsons^{3,4} · Martin Donnelley^{3,4}

Received: 28 January 2022 / Revised: 11 May 2022 / Accepted: 13 May 2022 / Published online: 2 July 2022
© The Author(s) 2022

Abstract

Purpose The rate of mucociliary transit (MCT) is an indicator of the hydration and health of the airways for cystic fibrosis (CF). To determine the effectiveness of cystic fibrosis respiratory therapies, we have developed a novel method to non-invasively quantify the local rate and patterns of MCT behaviour in vivo by using synchrotron phase contrast X-ray imaging (PCXI) to visualise the MCT motion of micron-sized spherical particles deposited onto the airway surfaces of live mice.

Methods In this study the baseline MCT behaviour was assessed in the nasal airways of *CFTR*-null and normal mice which were then treated with hypertonic saline (HS) or mannitol. To assess MCT, the particle motion was tracked throughout the synchrotron PCXI sequences using fully-automated custom image analysis software.

Results There was no significant difference in the MCT rate between normal and *CFTR*-null mice, but the analysis of MCT particle tracking showed that HS may have a longer duration of action in *CFTR*-null mice than in the normal mice.

Conclusion This study demonstrated that changes in MCT rate in CF and normal mouse nasal airways can be measured using PCXI and customised tracking software and used for assessing the effects of airway rehydrating pharmaceutical treatments.

Keywords Cystic fibrosis (CF) · Mucociliary transit (MCT) assessment · Automatic particle tracking · Synchrotron phase contrast x-ray images

1 Introduction

Cystic fibrosis (CF) is the most common recessive genetic disorder in the Caucasian population and is caused by dysfunction of the cystic fibrosis transmembrane conductance regulator (*CFTR*) gene and its associated CFTR protein, an epithelial ion channel [1]. The mucociliary transit (MCT) system consists of cilia—tiny hair-like structures that beat in a coordinated fashion inside the airway surface liquid (ASL) layer—to clear particulates and pathogens that are inhaled

and land on the airway surface. The *CFTR* ion channel defect causes dehydration of the airway surface liquid (ASL) and the production of thick, sticky mucus. Mucus obstruction in turn causes a cycle of lung infection and inflammation that gradually destroys the lung tissue. CF lung disease starts in childhood and dramatically decreases the quality and length of life [2].

Some current clinical CF treatments are designed to restore airway surface hydration by osmotically increasing the depth of the ASL and improving MCT. For instance, inhaled hypertonic saline (HS) has been shown to transiently and acutely increase MCT in both CF and normal patients [3, 4]. Similarly, inhaled mannitol is also clinically effective for producing an osmotic gradient on the surfaces of epithelial cells [5, 6]. Clinical assessments and treatments for CF disease are conducted indirectly due to the scarcity of methods to measure MCT activity in vivo. Traditionally, MCT quantification has been performed using inhaled radio-labelled, fluorescent, or radiopaque particles that are deposited in the airways [7–10]. However, these methods typically only investigate bulk particle clearance along airway surfaces and cannot elicit information about local MCT

✉ Hye-Won Jung
hyewon.jung@mymail.unisa.edu.au

¹ Science, Technology, Engineering and Mathematics (STEM), University of South Australia, Adelaide, SA 5001, Australia

² School of Physics and Astronomy, Monash University, Clayton, VIC 3800, Australia

³ Respiratory & Sleep Medicine, Women's and Children's Hospital, Adelaide, SA 5006, Australia

⁴ Robinson Research Institute and Adelaide Medical School, University of Adelaide, Adelaide, SA 5005, Australia

physiological effects that contribute to the bulk changes. To overcome this limitation, the effects of rehydrating treatments are typically observed in excised sections of airway epithelium because there are few methods that can examine or quantify the MCT rate in intact airways [11].

To directly assess the effect of CF treatments, we have developed a novel method to non-invasively measure MCT behaviour by dynamically tracking the behaviour of deposited particles along the airway surfaces during and after treatment [12–14]. These micron-sized particles allow MCT activity to be visualised in live anaesthetised animal models using synchrotron propagation-based phase contrast X-ray imaging (PCXI) [15–17]. The primary advantage of this approach is that it has the spatial and temporal resolution to visualise the behaviour of individual particles, and to measure local variations in MCT [18]. PCXI was utilised to examine the baseline MCT behaviour in the nasal airways of live anaesthetised normal and *CFTR*-null mice, and measure responses to HS or mannitol treatment. *CFTR*-null mice do not have a severe lung phenotype like that in humans, however their nasal epithelium does mimic the electrophysiological profile of human CF airways, and can therefore be used for testing the efficacy of therapeutic agents [19, 20]. A previous analysis of this dataset utilised a manual analysis performed by a single operator, to track the motion of the deposited particles throughout the image sequences [13]. However, the manual analysis involved the operator manually selecting and tracking a small number of moving particles that could be clearly identified (all stationary particles were excluded) and was an extremely time-consuming task. That analysis showed there were no statistically significant differences in MCT rate between the normal and CF mice [13], which agreed with previous studies examining MCT by *in vivo* microdialysis recordings of dye transport [8]. Nonetheless, due to the limitations of the analysis methods, it was hypothesised that this could have been due to the inability to manually track large numbers of marker particles.

Automatic detection and tracking of the MCT marker particles *in vivo* is an obvious goal but has been associated with a range of challenges. Particle detection difficulties can be exacerbated by noise, poor contrast between the background and particles, background motion between frames, and the presence of many particles that overlap with each other, and the complicated background anatomy [21, 22]. Furthermore, the uniformity of the particles (size, shape and greyscale level in the image), especially when many are clustered together, leads to analytical difficulties for tracking individual particles [23, 24]. Therefore, we have developed an automated particle detection and tracking method suitable for tracking MCT marker particle motion in PCXI images [25–27]. With this approach we propose that our experimental analysis can contribute to identifying disease-modifying interventions for CF lung diseases in

small animal models and enhance the development of new pharmaceutical treatments.

The aim of this research was to reanalyse the previously acquired dataset using our automated tracking methods, to non-invasively measure the baseline MCT activity in the nasal airway surfaces of live normal and *CFTR*-null mice. We also sought to quantify the changes in MCT activity produced by two common clinical CF aerosolised treatments, HS and mannitol. The present study performed particle tracking, and analysis of the particle dynamics using our previously-described custom-designed MCT analysis software [25–27].

2 Methods

2.1 X-Ray Imaging Setup

Imaging experiments were conducted on the BL20XU beamline at the SPring-8 synchrotron radiation facility in Japan. The PCXI setup for capturing time-lapse images was as previously described [12, 28]. All imaging was performed in the downstream experimental hutch 245 m from the light source, using 25 keV monochromatic X-rays. A sample-to-detector (i.e. propagation) distance of ~0.8 m was chosen to visualise a sufficiently strong bright-dark phase contrast fringe on the edge of each particle. The image field of view was 1.43 mm × 1.2 mm (2560 × 2160 pixels), and exposure times of 10 ms were used to reduce a motion blur and to produce a high signal to noise ratio. Images were acquired at 5 Hz.

2.2 Animal Procedures

All imaging was performed under approvals from the Animal Ethics Committees of SPring-8, the Women's and Children's Hospital, and the University of Adelaide. Experiments were performed in accordance with relevant guidelines and regulations, and reported according to the ARRIVE Essential 10 guidelines. A total of 25 normal C57Bl/6 (all female) and 24 CF FABp mice (10 male, 14 female) were utilised for imaging [28]. Mice were bred at the Women's and Children's Hospital in Adelaide and shipped to SPring-8 for the imaging experiments. Mice were randomly assigned to a treatment group, and anaesthetised with 100 mg/kg *i.p.* pentobarbital (64.8 mg/ml, Somnopenyl, Kyoritsu Seiyaku Corporation, Japan). The fur around the imaging area was removed to minimise interfering phase effects from hair in the images, and animals were secured in a custom-designed restraint and positioned in the imaging radiation enclosure such that the X-ray beam passed through the nasal respiratory epithelial tissue at the tip of the nose. Immediately prior to baseline imaging, spherical 20–30 µm uncoated

high refractive index (HRI) glass beads (Corpuscular, USA) were insufflated into the right nasal airway using a Dry Powder Insufflator™ (PennCentury, USA), with the delivery tip placed ~1 mm outside the nostril.

After baseline imaging to establish the MCT characteristics of the CF and normal mice prior to treatment, one of two treatments were delivered to the nasal airway, with mice randomly assigned to the treatment groups. HS was delivered using an Aeroneb nebuliser (Aerogen, Ireland) set to aerosolise for 45 s over the mouse nose. In contrast, dry mannitol powder (Pharmaxis, Australia) was delivered to the right nostril using a similar technique as for bead delivery. The Dry Powder Insufflator™ was actuated remotely (~5 s into the 1 min imaging block) from outside the imaging hutch using a hydraulic actuation mechanism to allow simultaneous delivery and imaging. Imaging then continued, with analysis performed for 12 min. Each mouse received a single treatment and was humanely killed at the end of the imaging period.

2.3 MCT Tracking

The primary outcome measures were the MCT rate and number of moving particles. MCT assessment was performed by automatically tracking particles using custom-designed software [27] designed to enable reliable detection and tracking of multiple uniform particles that were scattered across the low contrast PCXI images. This software was written in Matlab R2018 (The Mathworks), and was based on the previously described Jung method [25] that could identify circular shapes using a process termed “edge projection into the ring boundary” combined with a convolutional neural network (CNN) to improve detection accuracy. For particle tracking, a new multi-object tracking method was developed to correctly assign the corresponding particles to tracks, which relied on the confidence model that computes appearance and neighbouring topology affinity. Here, these discriminative components are learned by linear

discriminant analysis (LDA). This software also provides a detection recovery method using multi-frame association to “retrieve” any missing particles. To ensure robust tracking, the algorithm was set to track only those particles moving slower than ~25 mm/min. MCT measurements from the first frame of the tracking results of each trajectory that links two imaging blocks were also excluded, to avoid tracking jumps caused by the large inter-frame interval between blocks (see Fig. 1). Heat maps were produced as previously described [15, 29], and plotted the instantaneous velocity of every particle in every frame at each timepoint.

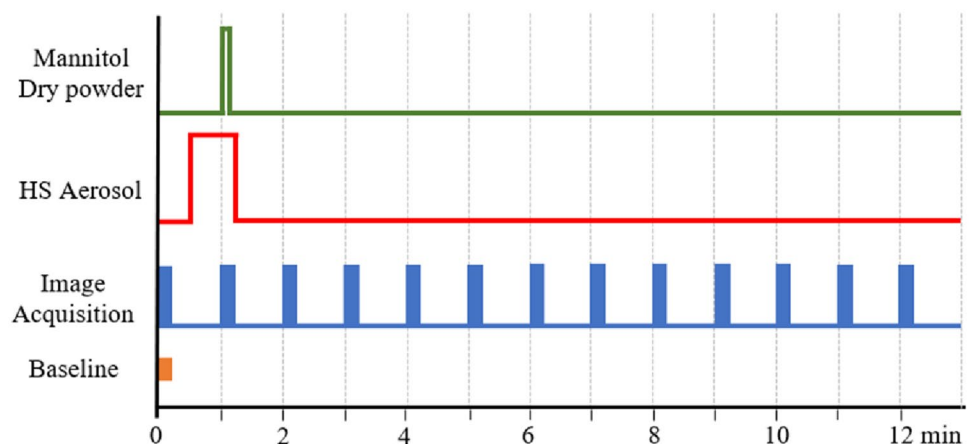
2.4 Statistical Analysis

All statistical analysis was performed using GraphPad Prism 8. Data was reported as mean \pm SD. Statistical significance was set at $p = 0.05$ and power ≥ 0.80 . Data normality was assessed with a Shapiro–Wilk test and when data failed normality assumptions, nonparametric methods were utilised. Baseline pre-treatment data is reported as CF vs normal. So that the MCT variability could be visualised and quantified, a nested table of all the replicate measures of the average MCT rate of every tracked particle was constructed and analysed with a nested t-test. The number of tracked particles and moving particles at baseline were assessed with unpaired Mann–Whitney tests. To assess the treatment effects over time, a 2-way (genotype \times treatment) repeated measures ANOVA was performed, with multiple comparisons using a Tukey post-hoc test. The same test was also used to analyse the total number of tracking particles and the number of moving particles.

3 Results

Anaesthetised normal ($n = 25$) and *CFTR*-null ($n = 24$) mice were imaged on the BL20XU beamline at the SPring-8 synchrotron radiation facility in Japan [28]. Uncoated 20–30 μm

Fig. 1 The experimental image acquisition and analysis plan. Images were acquired at 5 Hz in 15 s blocks (blue bars) each minute, so that each block has 75 images. After baseline imaging (orange marker), an aerosol treatment of hypertonic saline (HS) was delivered for 45 s (red bar), or mannitol was delivered as a dry powder (green bar)



high refractive index (HRI) glass bead MCT tracking particles were delivered to the nasal airways. Motion of the HRI beads along the airway surfaces was then imaged using a 1.43 mm × 1.2 mm field of view and 10 ms exposures at 5 Hz. After baseline imaging, the effects of aerosolised hypertonic saline or dry mannitol powder delivery were assessed over a 12 min imaging period.

Owing to technical challenges associated with remote monitoring and imaging, images were successfully acquired from 20 normal and 21 CF mice, with the number allocated to each group shown in Table 1. Here, the denominator and numerator in the third row indicate the total collected datasets and successful image datasets, respectively. An experiment was regarded as successful if the background anatomy did not move substantially throughout the imaging period, and if the HRI marker particles could be tracked properly by the software. An experiment was typically deemed unsuccessful if there were too many HRI marker particles in the airways for clearance to occur naturally, which happened because the particle insufflation procedure was highly variable. From the successful data sets, several test sets were selected for analysis, as shown in the “Test Sets” row. This was necessary because in many cases the bulk of the particle motion was barely discriminated by the human eye due to many particles severely overlapping each other, not moving at all, or moving too fast. The test sets were not evenly split across the two treatments, with fewer suitable test sets within the mannitol treatment group because many sets showed little particle movement in the assessed period.

3.1 Particle Tracking Results

Our particle tracking and analysis software was used to measure MCT activity [25, 26]. This software automatically identifies individual particles and tracks their dynamics throughout the time-lapse PCXI sequences. By utilising this tool, the time and manual effort required to perform MCT analysis was dramatically reduced, i.e., typically it took > 14 full days for a single operator to manually track the moving particles in a very small subset of the acquired images. In contrast, it took the automated algorithm ~ 10 h (unsupervised) to detect and track hundreds of moving and stationary particles, and to generate the visualisations for

each complete test set of over 900 images. Some particles exhibited very high velocities between frames, likely due to unpredictable bulk surface-fluid movement (typically from the addition of HS aerosol) suddenly transporting particles rapidly along the airway surface. To sustain the tracking robustness the algorithm was set to track only those particles moving slower than ~ 25 mm/min. This threshold was chosen to minimise the tracking errors of the tracking algorithm and was approximately the maximum speed at which the particle motion could be manually tracked by the human eye in these image sequences. Any particles moving faster than this would likely be due to bulk fluid movement rather than MCT. To be able to reduce this threshold it would be necessary to increase the field of view, but this would likely make particle detection and tracking much more challenging.

Figure 2 shows examples of the trajectory of each individually tracked particle in normal and CF mouse nasal airways following treatment with HS or mannitol. Each trajectory starts during the baseline imaging period and includes the period of faster particle movement produced by the treatment delivery. The motion of the particles is challenging to adequately visualise in static images such as Fig. 2 and is therefore shown more clearly in the supplementary videos (see Additional files: NH, NM, CH and CM). Here, the colour of each trajectory represents its confidence value, which was measured by an association function between each particle and trajectory; red represents the highest confidence and blue the lowest. Whenever the tracking algorithm “lost” the location of a particle its confidence coefficient was reduced, and its track gradually turned from red to blue. Finally, a blue trajectory disappears when that particle is “missing” for the maximum number of continuously missing frames (in this analysis this parameter was set to three frames).

As expected, the motion of the deposited MCT particles rapidly increased after treatment delivery. Unlike the trachea which has an almost cylindrical shape, the mouse nasal airway is anatomically complex and consists of bone, cartilage and three-dimensional folds of tissue containing different types of epithelium [30, 31]. This anatomy is superposed by the X-ray beam, and thus cannot be clearly identified in these two-dimensional projection images. Thus, when the particles were deposited, they landed on multiple surfaces within a complex nasal airway topography. Accordingly, the direction and speed of particle motion in two-dimensions can appear unpredictable and non-linear, i.e., some particles did not move while others were transported rapidly, likely because they were located in different anatomical regions.

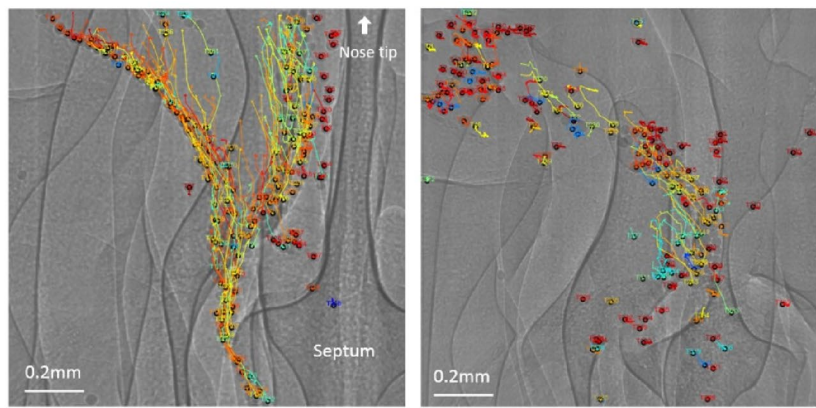
3.2 Baseline MCT Analysis

To quantify whether genotype affects MCT in the absence of any treatment, the MCT rate, the number of tracking particles, and the number of moving particles was

Table 1 The number of animals in each experimental group

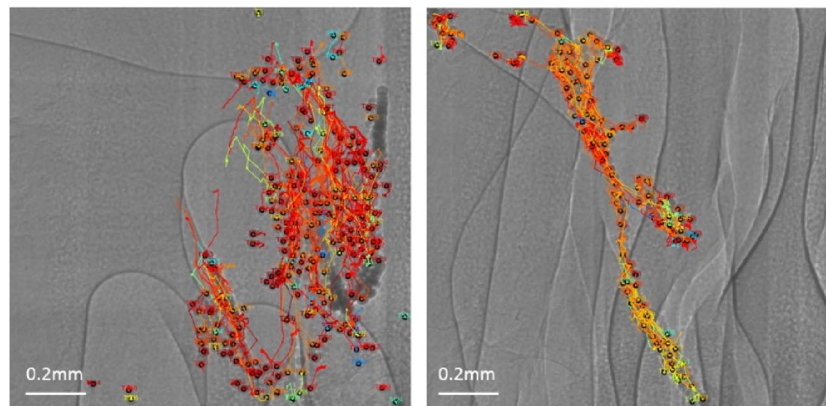
Mice	Normal C57Bl/6		CF FABp	
	HS	Mannitol	HS	Mannitol
Treatments				
Success/total experiments	9/11	11/14	10/13	11/11
Test sets	5	3	5	3
Group name	NH	NM	CH	CM

Fig. 2 Examples of particle tracking results in live mouse nasal airways following treatment with hypertonic saline (HS) or Mannitol. Red represents higher tracking confidence and blue represents lower tracking confidence



(a) Normal_HS at 1 minute

(b) Normal_Mannitol at 2 minutes

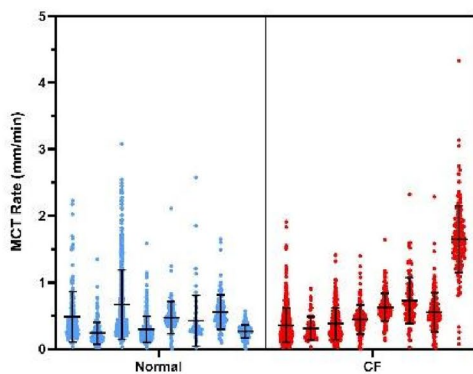


(c) CF_HS at 2 minutes

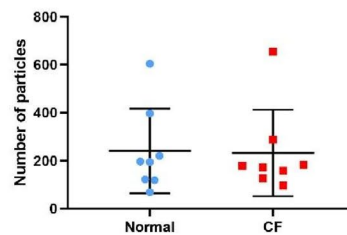
(d) CF_Mannitol at 1 minute

examined. Figure 3 shows an analysis of the baseline MCT behaviour. The mean MCT rate of the normal animals was 0.45 ± 0.39 mm/min and the CF animals was 0.56 ± 0.48 mm/min. A nested t-test showed that there was

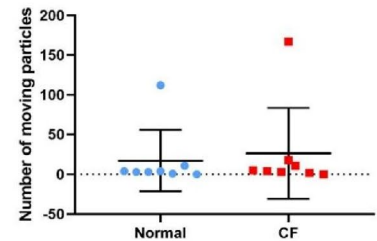
no statistically significant difference between the (untreated) normal and CF mouse nasal MCT. However, there were some statistically significant differences between the individual animals within these groups, suggesting a high level



(a)



(b)



(c)

Fig. 3 Baseline analysis (i.e. before any treatment was delivered), showing **a** the MCT rate, **b** the number of tracking particles and **c** the number of moving particles. Data presented as Mean \pm SD. Nested

or standard t-tests showed that no statistically significant differences were detected in any parameter at baseline

of variability was present even at baseline. The measured MCT rates are made up of three components: (1) The true particle movement due to MCT; (2) Low-level movement of the background due to the mouse respiratory or muscle motions (see supplementary videos for an example of this); and (3) A small number of tracking and association errors (approximately 7%) introduced by the algorithm confusing the identity of the particles [27]. Although not significant, the baseline MCT rate in the CF animals was higher than the normal group, and we attributed this to more frequent background motion in those animals. Figure 3b shows that the number of MCT tracking particles detected by the algorithm at baseline was the same in each group (mean number was 240 ± 177 for the normal mice and 232 ± 180 for CF). Since the particles were detected and tracked even if they did not move (unlike the previous manual analysis that only included particles that were identified as moving by the analyst), the number of tracked particles nearly equals the number of particles in an image, and is reduced only by untracked particles that overlapped each other. Figure 3c shows the number of particles that were moving faster than 1.1 mm/min (5-pixels per frame). This threshold was selected to exclude stationary or slowly moving particles, which included those moving less than the average 5-pixel background translation per frame that resulted from the mice breathing, and illustrates that only a small number of particles move rapidly at baseline. The addition of this threshold reduced the average number of tracked particles to 17 ± 38 for the normal mice and 26 ± 57 for the CF mice. There were no significant differences between the number of moving particles in each genotype. Note that Fig. 3b and c show that the normal and CF groups each contained one outlier animal that had a larger total number of particles and moving particles. This was likely caused by larger background motion in those animals, and could conceivably increase the measured MCT rate.

3.3 Effects of Treatments on MCT

The effects of treatments on the CF and normal mice were then investigated by examining the post-treatment MCT rate for each group using a 2-way repeated measures ANOVA and Tukey post-hoc test. There was a 2-way interaction between treatment type and time ($p < 0.001$) and a main effect of time ($p = 0.038$), but there were no other significant interaction effects. The change in MCT activity in all groups over time is shown in Fig. 4a, where the values at 0 min correspond to the baseline measurements presented in Fig. 3. The overall MCT rates increased in the nasal airway in the minutes following treatment delivery for both treatment types, but more so for the HS groups. The highest average MCT rate in this study was measured as 1.62 ± 0.82 mm/min (1 min) in the Normal_HS group and 1.37 ± 1.0 mm/min (5 min) in the CF_HS group. For most animals the MCT rate following aerosolised HS treatment returned to baseline levels after around 8 min. We found that the response durability to HS treatments was different between the normal and CF mice. The maximum MCT rate in the normal group that was treated with HS (Normal_HS) occurred at 1-min post-delivery and returned rapidly toward the baseline level. However, the higher MCT rate persisted for ~ 7 min longer in the CF group that was treated with HS (CF_HS). The mannitol treatment group did not show the variations in MCT rate that was present in the HS group.

For the total number of tracking particles, the same pattern emerged. There was a 2-way interaction between treatment type and time ($p < 0.01$), a main effect of time ($p = 0.0033$), but no other significant interaction effects. In Fig. 4b, the large number of particles that were observed during the baseline imaging gradually reduced in number over time and this measure more obviously shows the difference in the normal and CF groups treated with HS. At 7 to 12 min post-delivery the number of particles in the normal

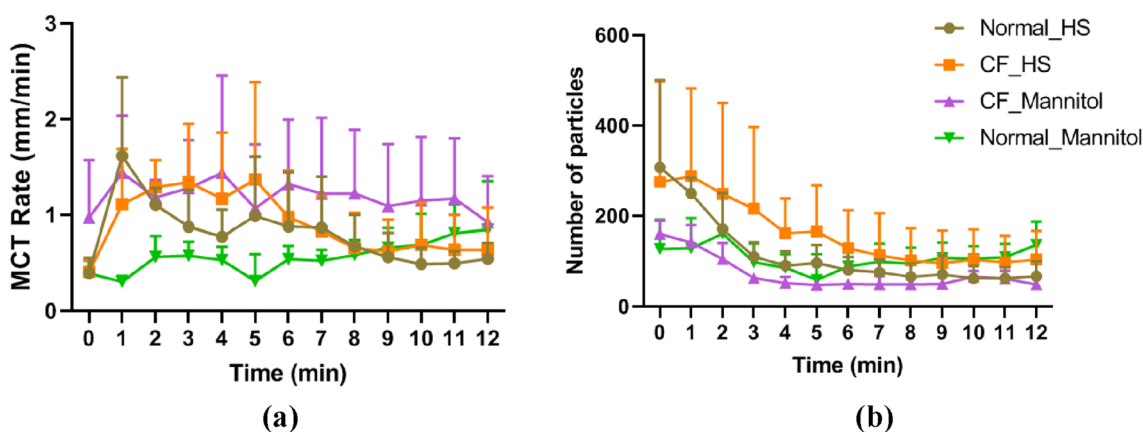


Fig. 4 Time-course analysis of the behaviour of all stationary and moving MCT tracking particles. **a** The MCT rate and **b** the total number of tracking particles tracked. Data presented as Mean \pm SD

mice treated with hypertonic saline was significantly lower than the 1-min timepoint (7–9 min: $p < 0.05$; 10 and 12 min: $p < 0.01$; 11 min: $p < 0.001$).

Given that the presence of many stationary particles skews the mean MCT rate and leads to difficulties in comparing MCT effects across experiments, we also analysed the data for only those particles moving faster than an average of 1.1 mm/min (as described above). For the MCT rate there was a main effect of time, but no interactions. For the number of moving particles there was a 2-way interaction between treatment type and time ($p = 0.007$), a main effect of time ($p = 0.024$), but no other significant interaction effects. These effects can be identified more clearly in Fig. 5 where only moving particles are included. The highest MCT rates were measured as 3.51 ± 0.79 mm/min (1 min) in the Normal_HS group and 3.1 ± 0.72 mm/min (1 min) in CF_HS group (Fig. 5a). Note that these MCT rates should

be examined in combination with the graphs of the number of moving particles. Interestingly, Fig. 5b shows that the number of moving particles remained higher for longer following treatment with HS, and that this also returned to close to baseline after ~8 min.

3.4 Particle Velocity Analysis

To better visualise the velocity (the magnitude and direction) of all the particles, a two-dimensional heat-map displaying the direction and instantaneous speed of the particle trajectories is shown in Fig. 6. At baseline (0 min), the bulk of particles remain at the origin because most are stationary. The overall MCT rate of particles transiently increases after HS treatment delivery (1 min), and then gradually return toward baseline. As shown in Figs. 4 and 5, the more diverse range of MCT rates in the CF mice treated with HS aerosol

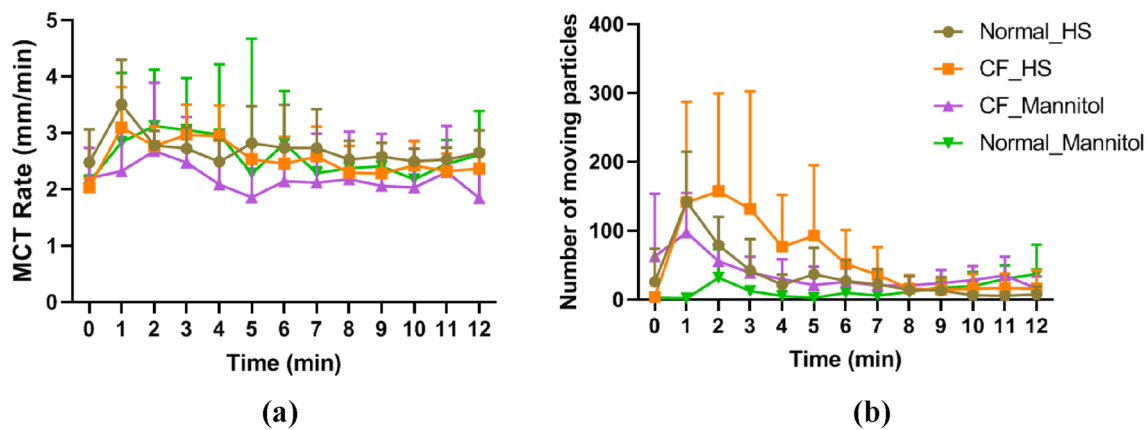


Fig. 5 Time-course analysis of the behaviour of all MCT tracking particles that were moving faster than the 1.1 mm/min threshold. **a** The MCT rate and **b** the number of moving tracking particles tracked. Data presented as Mean \pm SD

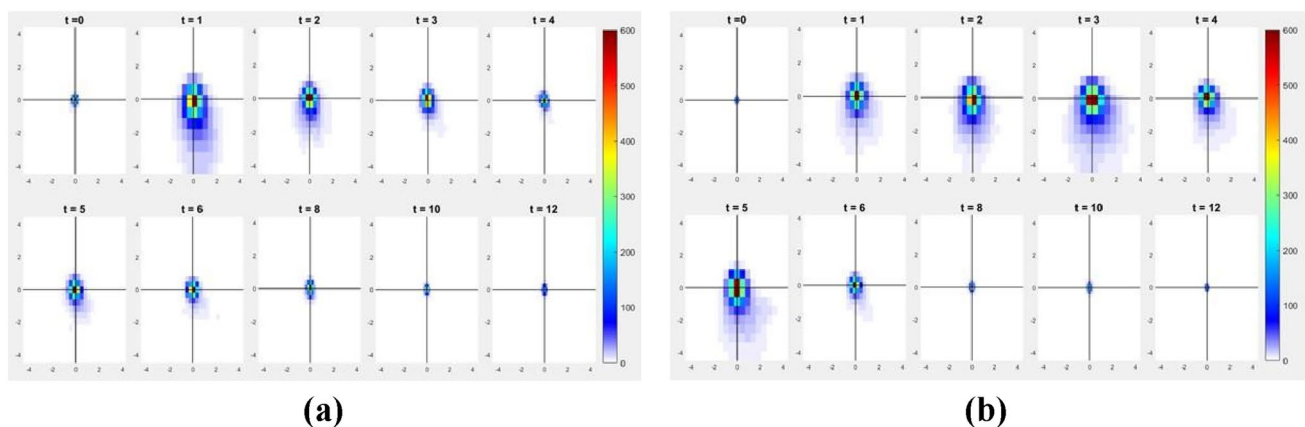


Fig. 6 Two-dimensional heat-map of the MCT velocity in **a** normal mice and **b** CF mice shows the effect of HS aerosol treatment delivery at each time point. Magnitude toward the angular direction is represented by the colour map. Stationary particles are located at

the origin and fast-moving particles are further from the origin. The direction of the heat-map represents the predominant direction of motion of the tracked MCT particles

(see Fig. 6b), compared with the normal group (Normal_HS) can be identified up to 6 min post-treatment. Variability in the direction of motion is also apparent, and likely reflects the deposition of particles onto different locations within the complex three-dimensional nasal anatomy already noted (see supplementary videos). The mannitol treatment group is not shown using this heat-map presentation due to the small number of moving particles over time.

4 Discussion

This research has demonstrated that MCT behaviour along the airway surface can be examined by automatically tracking the motion of deposited spherical MCT marker particles using synchrotron PCXI. Here we found that the baseline MCT rates were similar to those determined in the manual analysis (0.33 mm/min for the normal mice and 0.49 mm/min for the CF mice) [13], but these were all lower than those previously reported by Grubb et al. [8] who found mean MCT rates of 2.2 mm/min for normal mice and 2.3 mm/min for CF mice. However, in their analysis the addition of the dye to the airway likely increases airway surface hydration, and therefore increases MCT. Our analysis was undertaken in a low humidity X-ray imaging enclosure, which may have reduced nasal MCT. Furthermore, the mass and shape of the individual HRI particles may have been responsible for a lower measured MCT rate compared to the dissolved-dye transport method employed by Grubb et al., meaning that these two methodologies are not directly comparable [8]. Nonetheless, in this automated analysis at baseline the algorithm tracked on average 200 fold larger number of particles than the manual analysis [13] (2.33 particles/mouse for normal and 2.25 particles/mouse for CF), demonstrating a substantial benefit of the automated tracking method.

The mean post-treatment MCT rates were lower than those measured manually in our previous analysis of this data set [13], because the automated algorithm was able to identify and track a very large number of stationary particles, the presence of which reduced the mean MCT rate significantly. We hypothesise that when the particles are delivered to the nasal airway using the dry powder insufflator they land on different types of epithelium (respiratory, squamous, transitional), which likely alters the rate at which the particles move (e.g., squamous epithelium does not possess an MCT-like transport mechanism), meaning that some particles can remain stationary throughout. Hence, we investigated the MCT rates in the moving particles (over 1.1 mm/min). This still resulted in lower MCT rates than our previous analysis, due to the presence of a large number of slowly moving particles that were not identified as moving in the manual analysis. Parity could likely be achieved by

increasing this threshold further. Unsurprisingly, the number of tracking particles decreases over time, likely because particles leave the field of view due to MCT action towards the tip of the nose. Relatively few particles enter the field of view from deeper in the nose because the insufflator does not deliver many particles deeper than this.

In all of our analyses there was no genotype interaction. This agrees with previous studies [8, 13], and suggests that while electrophysiological differences in this CF mouse nose can be measured, particle clearance is not affected. However, the time \times treatment interactions we did find suggest that the strength and duration of action for HS treatments appears to be different to mannitol: The normal mice responded quickly to the HS treatment, and the peak of MCT activity was observed at 1 min and dropped off rapidly. For the CF mice, the effects lasted for \sim 7 min longer and came back to the baseline after 8 min. Mannitol produced a more consistent effect than HS, with higher rates and numbers of moving particles than HS toward the end of the study period. Only a few experimental samples (5 out of total 22 mice) in the mannitol treatment groups showed movement that could be detected by the automated particle analysis algorithm. This suggests that the mannitol treatment had less of an effect on MCT activity during the imaging period because it may result in a short exposure duration of the treatment. It is possible that the differences between these two groups were driven primarily by the different composition of the treatment, with the liquid in the HS formulation providing rapid hydration in contrast to the dry powder formulation of the mannitol. Furthermore, some bias may have been introduced by the exclusion of test sets containing limited motion, most of which came from the mannitol group. Nonetheless, the high variability of the MCT behaviour we measured suggests that additional studies would be valuable, with sample sizes able to be calculated using the variability values we have reported here.

Even though synchrotron PCXI can effectively visualize the MCT behaviour in the nasal airway, the automated tracking software faces several challenges. (1) Many of the datasets captured during this experiment were not useful because most particles were stationary or exhibited negligible movement over the imaging period. In more recent studies we have demonstrated that the particle surface coating is important for determining how the particles are cleared by MCT in ex vivo tracheal samples from rats [32]. A proportion of the uncoated HRI particles in the present study likely became stuck in the mucus in the nose, and therefore could not be cleared. The use of COOH coated particles would likely alter this behaviour and should be considered for future studies [32]. The relatively large particle size may have also affected clearance behaviour, and this should be assessed in future PCXI studies. (2) Some datasets contained many particles that overlapped with each other and confounded

the analysis (these datasets could not be manually analysed either). A more controllable method of accurately depositing the correct number of tracking particles into the nasal airway is required to ensure that the MCT system is not overwhelmed by a large particle load, and to enable automated particle tracking to be performed. (3) Background motion due to respiration and other muscle movements makes tracking challenging. To enable the 1.1 mm/min threshold to be reduced, better anaesthetic regimens could be used (e.g. medetomidine, butorphanol and midazolam rather than sodium pentobarbital [28]) to reduce motion, and background image registration algorithms could be used. The challenge with these is that the tracking particles are often the strongest landmarks in the image. (4) Tracking and analysis of very fast-moving particles was challenging due to the difficulties in associating multiple particles with identical appearance in adjacent frames when they have moved a long distance. As noted in our previous study, this problem exists for manual tracking also. Further studies are therefore needed to determine the impact of the “untrackable” particles on the analysis outcomes, although only a small number of particles could not be automatically tracked. With further improvement of the imaging system to enable image capture at higher frame rates, and the use of a larger field of view, this system could provide more robust tracking performance. In addition, while synchrotron facilities are not available to all researchers, laboratory-based approaches are becoming available. Propagation-based PCXI of the respiratory system in small animals is now possible with liquid–metal-jet anode electron-impact x-ray sources [33] and compact light sources [34], although the resolutions required for MCT assessment remain hard to achieve.

5 Conclusion

Synchrotron PCXI can be utilised for in vivo nasal MCT rate analysis in small animals, and these experimental methods now permit a detailed understanding of how MCT rates change in response to administered therapies. This paper describes the outcomes from applying our software based MCT rate measurements to normal and CF mice, by detecting and tracking the motion of deposited tracking particles over hundreds of images. Our results show that there was no significant difference in MCT rates between the normal and CF mouse nasal airways, but the persistence of effect following HS treatment delivery was more obvious in CF mice than normal mice. Improvements to this non-invasive MCT imaging assessment should enable the rapid testing and quantification of the effectiveness of new therapeutic options targeted at increasing airway hydration and mucus clearance.

Supplementary Information The online version contains supplementary material available at <https://doi.org/10.1007/s40846-022-00718-3>.

Acknowledgements The synchrotron radiation experiments were performed on the BL20XU beamline at the SPring-8 synchrotron, with the approval of the Japan Synchrotron Radiation Institute (JASRI) under proposal number 2013A1706 and 2013B1734. We thank Naoto Yagi, Kentaro Uesugi, Yoshio Suzuki and Akihisa Takeuchi for their assistance at the BL20XU beamline, as well as Nigel Farrow, Richard Carnibella and Isobel Aloisio for their assistance during the experiments. Dr Wolfgang Jarolimek (Pharmaxis Ltd) provided the mannitol powder. Prof Andreas Fouras (Monash University) provided imaging advice and supplied essential experimental equipment including the sCMOS detector. 4D Medical provided the mouse ventilator system. The authors thank Dr Ivanka Prichard for providing statistical advice.

Author Contributions HJ, IL and SL analyzed the tracking results of particles based on their custom software and drafted the manuscripts. MD, DP and KM designed the studies, provided the PCXI data used in this paper, and drafted and critically revised the manuscript. All authors reviewed and approved the final manuscript.

Funding Open Access funding enabled and organized by CAUL and its Member Institutions. Studies were supported by the WCH Foundation, NHMRC Australia, philanthropic donors via the Cure4CF Foundation, and Pharmaxis Ltd. M.D. was supported by a Robinson Research Institute Career Development Fellowship, K.M. by an ARC DECRA during experiments and then an ARC Future Fellowship during writing. Travel was supported by the Australian Synchrotron International Synchrotron Access Program (ISAP). The ISAP is an initiative of the Australian Government being conducted as part of the NCRIS.

Open Access This article is licensed under a Creative Commons Attribution 4.0 International License, which permits use, sharing, adaptation, distribution and reproduction in any medium or format, as long as you give appropriate credit to the original author(s) and the source, provide a link to the Creative Commons licence, and indicate if changes were made. The images or other third party material in this article are included in the article's Creative Commons licence, unless indicated otherwise in a credit line to the material. If material is not included in the article's Creative Commons licence and your intended use is not permitted by statutory regulation or exceeds the permitted use, you will need to obtain permission directly from the copyright holder. To view a copy of this licence, visit <http://creativecommons.org/licenses/by/4.0/>.

References

1. Wine, J. J. (1999). The genesis of cystic fibrosis lung disease. *The Journal of Clinical Investigation*, 103(3), 309–312.
2. Cutting, G. R. (2015). Cystic fibrosis genetics: From molecular understanding to clinical application. *Nature Reviews Genetics*, 16(1), 45.
3. Elkins, M., et al. (2006). National Hypertonic Saline in Cystic Fibrosis (NHSCF) Study Group. A controlled trial of long-term inhaled hypertonic saline in patients with cystic fibrosis. *New England Journal of Medicine*, 354(3), 229.
4. Robinson, M., et al. (1997). Effect of increasing doses of hypertonic saline on mucociliary clearance in patients with cystic fibrosis. *Thorax*, 52(10), 900–903.
5. Flume, P. A., et al. (2015). Optimising inhaled mannitol for cystic fibrosis in an adult population. *Breathe*, 11(1), 39–48.

6. Mall, M. A., Danahay, H., & Boucher, R. C. (2018). Emerging concepts and therapies for mucoobstructive lung disease. *Annals of the American Thoracic Society*, *15*(Supplement 3), S216–S226.
7. Sousa, A. A. R., Fernández, J. M. B., Miller, J., & Mir-Montejano, M. (2019). Physiological study of pulmonary involvement in adults with cystic fibrosis through simulated modeling of different clinical scenarios. *Medical & Biological Engineering & Computing*, *57*(2), 413–425.
8. Grubb, B. R., Jones, J. H., & Boucher, R. C. (2004). Mucociliary transport determined by in vivo microdialysis in the airways of normal and CF mice. *American Journal of Physiology-Lung Cellular and Molecular Physiology*, *286*(3), L588–L595.
9. Donaldson, S. H., Corcoran, T. E., Laube, B. L., & Bennett, W. D. (2007). Mucociliary clearance as an outcome measure for cystic fibrosis clinical research. *Proceedings of the American Thoracic Society*, *4*(4), 399–405.
10. Hoegger, M. J., et al. (2014). Assessing mucociliary transport of single particles in vivo shows variable speed and preference for the ventral trachea in newborn pigs. *Proceedings of the National Academy of Sciences*, *111*(6), 2355–2360.
11. Ballard, S. T., Parker, J. C., & Hamm, C. R. (2006). Restoration of mucociliary transport in the fluid-depleted trachea by surface-active instillates. *American Journal of Respiratory Cell and Molecular Biology*, *34*(4), 500–504.
12. Donnelley, M., et al. (2014). Non-invasive airway health assessment: Synchrotron imaging reveals effects of rehydrating treatments on mucociliary transit in-vivo. *Scientific Reports*, *4*, 3689.
13. Donnelley, M., Morgan, K., Farrow, N., Siu, K., & Parsons, D. (2016). Non-invasive airway health measurement using synchrotron x-ray microscopy of high refractive index glass microbeads. In *AIP conference proceedings* (Vol. 1696, p. 020011). AIP Publishing.
14. Gardner, M., et al. (2020). Towards automated in vivo tracheal mucociliary transport measurement: Detecting and tracking particle movement in synchrotron phase-contrast X-ray images. *Physics in Medicine & Biology*. <https://doi.org/10.1088/1361-6560/ab7509>
15. Gradl, R., et al. (2018). In vivo dynamic phase-contrast x-ray imaging using a compact light source. *Scientific Reports*, *8*(1), 6788.
16. Wilkins, S., Gureyev, T., Gao, D., Pogany, A., & Stevenson, A. (1996). Phase-contrast imaging using polychromatic hard X-rays. *Nature*, *384*(6607), 335–338.
17. Martin, A. R., Thompson, R. B., & Finlay, W. H. (2008). MRI measurement of regional lung deposition in mice exposed nose-only to nebulized superparamagnetic iron oxide nanoparticles. *Journal of Aerosol Medicine and Pulmonary Drug Delivery*, *21*(4), 335–342.
18. Donnelley, M., Gardner, M., Morgan, K., & Parsons, D. (2021). Non-absorptive clearance from airways. In *Inhaled medicines* (pp. 197–223). Elsevier.
19. McCarron, A., Donnelley, M., & Parsons, D. (2018). Airway disease phenotypes in animal models of cystic fibrosis. *Respiratory Research*. <https://doi.org/10.1186/s12931-018-0750-y>
20. McCarron, A., Parsons, D., & Donnelley, M. (2021). Animal and cell culture models for cystic fibrosis. *The American Journal of Pathology*, *191*(2), 228–242. <https://doi.org/10.1016/j.ajpath.2020.10.017>
21. Smal, I., & Meijering, E. (2015). Quantitative comparison of multiframe data association techniques for particle tracking in time-lapse fluorescence microscopy. *Medical Image Analysis*, *24*(1), 163–189.
22. Feng, L., Xu, Y., Yang, Y., & Zheng, X. (2011). Multiple dense particle tracking in fluorescence microscopy images based on multidimensional assignment. *Journal of Structural Biology*, *173*(2), 219–228.
23. Wang, X., et al. (2016). Active colloids segmentation and tracking. *Pattern Recognition*, *60*, 177–188.
24. Rezatofighi, S. H., Gould, S., Vo, B. T., Vo, B.-N., Mele, K., & Hartley, R. (2015). Multi-target tracking with time-varying clutter rate and detection profile: Application to time-lapse cell microscopy sequences. *IEEE Transactions on Medical Imaging*, *34*(6), 1336–1348.
25. Jung, H.-W., Lee, S.-H., Donnelley, M., Parsons, D., & Lee, I. (2017). Automated detection of circular marker particles in synchrotron phase contrast X-ray images of live mouse nasal airways for mucociliary transit assessment. *Expert Systems with Applications*, *73*, 57–68.
26. Jung, H.-W., Lee, I., Lee, S.-H., Parsons, D., & Donnelley, M. (2017). Multiple mucociliary transit marker tracking in synchrotron X-ray images using the global nearest neighbour method. In *39th annual international conference of the IEEE engineering in medicine and biology society (EMBC)* (pp. 1824–1827).
27. Jung, H.-W., Lee, S.-H., Donnelley, M., Parsons, D., Stamatescu, V., & Lee, I. (2019). Multiple particle tracking in time-lapse synchrotron X-ray images using discriminative appearance and neighbouring topology learning. *Pattern Recognition*, *93*, 485–497.
28. Morgan, D. P. K., Cmielewski, P., McCarron, A., Gradl, R., Farrow, N., Siu, K., Takeuchi, A., Suzuki, Y., Uesugi, K., Uesugi, M., Yagi, N., Hall, C., Klein, M., Maksimenko, A., Stevenson, A., Hausermann, D., Dierolf, M., Pfeiffer, F., & Donnelley, M. (2019). Methods for dynamic synchrotron X-ray respiratory imaging of live animals. *Journal of Synchrotron Radiation*. <https://doi.org/10.1107/S1600577519014863>
29. Donnelley, M., Morgan, K. S., Awadalla, M., Farrow, N. R., Hall, C., & Parsons, D. W. (2017). High-resolution mucociliary transport measurement in live excised large animal trachea using synchrotron X-ray imaging. *Respiratory Research*, *18*(1), 95.
30. Herbert, R. A., Janardhan, K. S., Pandiri, A. R., Cesta, M. F., & Miller, R. A. (2018). Nose, larynx, and trachea. *Boorman's pathology of the rat* (pp. 391–435). Elsevier.
31. Mery, S., Gross, E. A., Joyner, D. R., Godo, M., & Morgan, K. T. (2016). Nasal diagrams: A tool for recording the distribution of nasal lesions in rats and mice. *Toxicologic Pathology*, *22*(4), 353–372. <https://doi.org/10.1177/019262339402200402>
32. Gardner, M., McCarron, A., Morgan, K., Parsons, D., & Donnelley, M. (2019). Particle coating alters mucociliary transit in excised rat trachea: A synchrotron X-ray imaging study. *Scientific Reports*, *9*(1), 10983.
33. Murrie, R. P., et al. (2020). Real-time in vivo imaging of regional lung function in a mouse model of cystic fibrosis on a laboratory X-ray source. *Scientific Reports*. <https://doi.org/10.1038/s41598-019-57376-w>
34. Gradl, R., et al. (2019). Visualizing treatment delivery and deposition in mouse lungs using in vivo x-ray imaging. *Journal of Controlled Release*, *307*, 282–291. <https://doi.org/10.1016/j.jconrel.2019.06.035>